Influence of impeller–tongue interaction on the unsteady cavitation behavior in a centrifugal pump

Article *in* Engineering Computations · March 2016

DOI: 10.1108/EC-09-2014-0179

Influence of impeller-tongue interaction on the unsteady cavitation behavior in a centrifugal pump

Received 24 October 2014
Revised 11 May 2015
Accepted 10 June 2015

Long Meng
College of Water Resources and Civil Engineering, China Agricultural University, Beijing, China
Min He
Shanghai Kaiquan Pump(Group) Co. Ltd, Shanghai, China
Lingjiu Zhou
College of Water Resources and Civil Engineering, China Agricultural University, Beijing, China
Jing Yang and Zhengwei Wang
Department of Thermal Engineering, Tsinghua University, Beijing, China, and
Bryan Karney
Department of Civil Engineering, University of Toronto, Toronto, Canada

Abstract

Purpose – The purpose of this paper is to analyze the cavitation dynamics in the blade channel of a centrifugal pump with a particular focus on the direct influence of the pump's volute.

Design/methodology/approach – A homogeneous multiphase model, namely the Zwart-Gerber-Belamri cavitation model, is employed to numerically describe the evolution of the process of cavitation within the pump. The RNG k-e turbulence model is applied to analyze the unsteady turbulent flow. A second order implicit formulation is used for the time discretization for the unsteady flow calculation and a finite volume algorithm is used for the space discretization.

Findings – The cavities in the passage exhibit an obvious life cycle which includes initiation, growth, contraction, and separation, and collapse with a frequency corresponding to the impeller rotation frequency under off-design conditions. This phenomenon arises through an alternating interaction between reverse flow with the cavity interface and is associated with the response of the vortex region to the effect of uneven pressure distribution on volute and impeller-tongue interaction.

Originality/value – This study simulated and analyzed the complex transient cavitation flow patterns inside a centrifugal pump and explains the reason for the unsteadiness. This knowledge is instructive in achieving the stable operation of pumps and in trouble shooting rough or cavitating operation.

Keywords Centrifugal pump, Cavity, Impeller rotating period, Impeller-tongue interaction, Uneven pressure distribution, Pump volume

Paper type Research paper

Conflict of interests: the authors declare that there is no conflict of interests regarding the publication of this paper.

The authors gratefully acknowledge the support from the National Natural Science Foundation of China (No. 51279205).

0264-4401
DOI 10.1108/EC-09-2014-0179

Nomenclature

H	head of the pump (m)	$NPSH$	net pressure suction head (m), $NPSH = \left((P_{in} - P_v)/(\rho g)\right) + \left(v_{in}^2/2g\right)$
Ho	head of the pump at the optimal point (m)	N_S	specific speed of the pump, $N_S = \left(N\sqrt{Q}\right)/(gH)^{3/4}$
N	rotation speed of the pump (rpm)	Q	flow rate (m^3/s)
P_{in}	pressure of the inlet (Pa)	Q_0	flow rate at the optimal point (m)
P_v	vaporization pressure under working temperature (Pa)	η	hydraulic efficiency of the pump
v_{in}	flow velocity of the inlet (m/s)		

1. Introduction

Cavitation in centrifugal pumps is a well-known phenomenon which usually results in substantial performance losses, strong unsteady forces, operational noise, low efficiency, impeller and volute erosion and premature maintenance (Coutier-Delgosha *et al.*, 2002). Many experiments have been done to investigate the physics of cavitation and also many numerical calculations have simulated cavity development and collapse inside pumps (Nwaoha, 2009; Mejri *et al.*, 2005, 2006; Li *et al.*, 2007; Coutier-Delgosha *et al.*, 2002; Dupont and Casartelli, 2002; Medvitz *et al.*, 2002). The inception of cavitation – that is, the threshold corresponding to a notable pump head drop – have also been measured and predicted. For example, Medvitz *et al.* (2002) captured the characteristic performance trends associated with off-design flow as well as the rapid drop in head coefficient at low cavitation numbers. Coutier-Delgosha *et al.* (2003) investigated the quasi-steady cavitating behavior of three pumps and successfully predicted the head drop and the cavity structures using the barotropic state law. However, above mentioned researches mainly focussed on the steady simulation, while in reality the interaction of the running impeller and the tongue may induce complicated and important unsteady phenomenon inside the pump. Niazi *et al.* (2010) also pointed out that any steady state solution will be unable to trace the growth, movement and collapse of bubbles. Unsteady simulation of cavitation is therefore crucial to the understanding of cavitation.

The unsteady simulation of cavitation has already been widely used for the prediction of cavitation characteristics of inducers and hydrofoils (Kobayashi and Chiba, 2009). Most of these studies indicated that the instability of cavitation is related to the changes in flow angle (Tani *et al.*, 2012), the flow rate and cavitation number (Pouffary *et al.*, 2008a), as well as the pressure gradient at cavity closure (Okita *et al.*, 2003). More particularly, the interaction between reversed flow and cavity interface (Wang *et al.*, 2001; Huang *et al.*, 2011; Watanabe *et al.*, 2009; Flores *et al.*, 2008; Hao *et al.*, 2010; Huang *et al.*, 2010, 2011; Pouffary *et al.*, 2008b) is identified to be a major factor causing the periodic break-up and shedding of the cavity, and thus has been investigated by many researchers. In the context of hydraulic machines, Xiao (Xiao *et al.*, 2010) used RANS based turbulence models to simulate the unsteady flow inside turbines, and the results agreed well with the experimental data.

The development of unsteady cavitation on impeller blades resembles that on a single hydrofoil in a cavitation tunnel to some extent. However, in the case of a single hydrofoil the cavitation dynamics is dominated by periodical, self-excited cloud generation and the frequency is closely related to the Strouhal number. By contrast, in the case of a centrifugal pump, the interaction between the impeller and the volute tongue often strongly influences cavity evolution due to the inevitable periodically

variation of the flow conditions in the impeller passage. This paper reports on three-dimensional unsteady cavitating simulations performed in a specific centrifugal pump configuration. Attention is paid to the influence of impeller-tongue interaction on the unsteady cavitation behavior inside the impeller channel.

2. Numerical simulation

2.1 Numerical method

The calculation model is a centrifugal pump with specific speed $N_S = 0.519$ and the rotational speed is $N = 2{,}900$ rpm. The computational mesh consists of unstructured hybrid grid. To ensure the mesh requirements of the turbulence model, a so-called prism grid was used to refine the mesh near the wall. The mesh near the leading and tailing edges and the tongue of the volute was also carefully refined, and the Y^+ near the impeller wall mesh is within 30~300. The grid is shown in Figure 1 (left). Grid convergence tests showed that a grid with 1,423,000 elements balanced the computational time and accuracy.

A velocity boundary condition is imposed at the inlet of the suction pipe and a uniform pressure is imposed on the outlet. At the solid wall, no-slip condition is enforced and a wall function is applied in all near-wall computation cells. In order to improve the rate of convergence and computational stability the initial pressure and flow field was set using a single phase (cavitation free) steady flow condition.

Several time steps (T/60, T/120, T/180 and T/360, where T is the period of revolution) were tested for a particular cavitating condition. It was found that a time step of T/120 gave strongly similar results to the smaller steps of T/180 and T/360. Thus, that time step was chosen for the production runs of the simulation program. The total duration for each simulation for each numerical run was taking as about $10T$. Within each simulation, the convergence precision for iterations was set to 10^{-4}.

Several numerical monitoring points were positioned in both suction side (ss1, ss2 and ss3) and pressure side (ps1, ps2 and ps3) of the blade for the unsteady study. These are shown on the right side of Figure 1.

2.2 Cavitation and turbulence models

The Zwart-Gerber-Belamri cavitation model (ANSYS CFX, Release11.0, 2012) (CFX), which is a homogeneous multiphase model, was used to describe the evolution of cavity. Bubble number density n is used by this model to calculate the total interphase

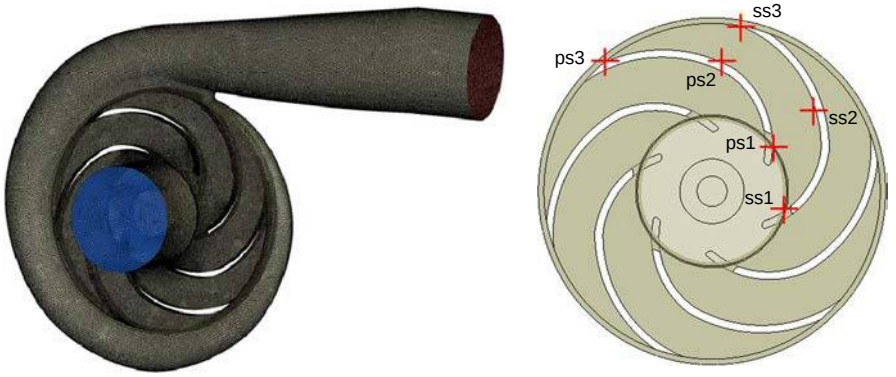

Figure 1.
Mesh(left) and monitoring points (right) inside the calculation domain

mass transfer rate in per unit volume, and the mass transfer rate of one bubble is:

$$R = n \times \left(4\pi R_B^2 \rho_v \frac{dR_B}{dt}\right) \tag{1}$$

The net mass transfer rate is expressed by:

$$R_e = F\frac{3\alpha\rho_v}{R_B}\sqrt{\frac{2|P_B - P|}{3}}\text{sign}(P_B - P) \tag{2}$$

where F is an empirical coefficient. An adjusted rate expression is needed for the two conditions of cavity growth and decay, depending on the local pressure.

If $P \leqslant P_v$:

$$R_e = F_{vap}\frac{3\alpha_{nuc}(1-\alpha_v)\rho_v}{R_B}\sqrt{\frac{2(P_v - P)}{3\rho_l}} \tag{3}$$

If $P \geqslant P_v$:

$$R_c = F_{cond}\frac{3\alpha_v\rho_v}{R_B}\sqrt{\frac{2(P - P_v)}{3\rho_l}} \tag{4}$$

The empirical constants were set as $F_{vap} = 50$, $F_{cond} = 0.01$. The inception diameter for the cavity is set at $R_B = 2 \times 10^{-6}$ m, and the nucleation site volume fraction is set at $\alpha_{nuc} = 5 \times 10^{-4}$.

The RNG $k-\varepsilon$ turbulence model is applied for the unsteady turbulent flow. This model is well suited for dealing with flows having a high strain rate and large streamline curvature. When flows are expected to have large scale flow separation, this model will is expected to perform well. A second order implicit formulation is used for the unsteady temporal discretization and a finite volume algorithm for the spatial discretization within the numerical simulation. A second order central difference scheme is used for the source terms and a second order upstream difference for the convective terms.

2.3 Comparison between simulation and tests data

Cavitating flows were simulated for a range of discharges as a fraction of Qo, the flow rate at the optimal efficiency point (0.46Qo, 0.7Qo, 1.0Qo and 1.3Qo). The head-σ and efficiency-σ curves were obtained by reducing the pump outlet pressure. As expected, a decrease of the *NPSH*, causes the pump head H and efficiency to initially remain constant; but after a certain *NPSH* is reached, the head H and efficiency η drops sharply, as shown in Figure 2(a)-(b). Some typical conditions for flow rate 0.7Qo were investigated (labeled in Figure 2(a)): Cond. A, Cond. B, Cond. C, Cond. D and Cond. E correspond to non-cavitation case, the inception cavitation point, the point just before the sudden head drop, the point of 3 percent head drop (critical point) and a point of serious cavitation, respectively. These points are labeled in Figure 2(a).

Test data are presented in Figure 2. It can be seen that the predicted tendency agree closely both qualitatively and quantitatively with the experiment ones. Although there are some small differences, the point before the sudden head drop and the critical point are in close accordance in all cases. This confirm the reasonableness of cavitating simulation and the associated turbulence model.

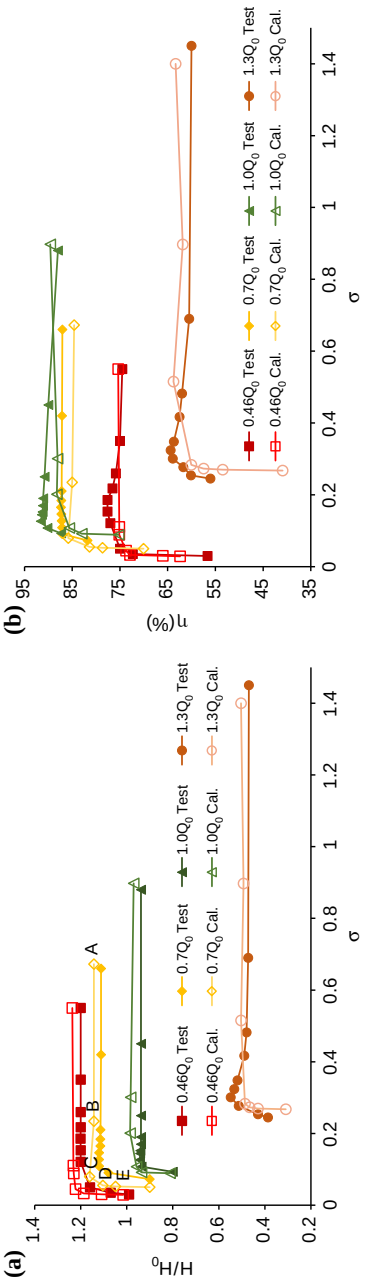

Figure 2.
The head-σ and efficiency-σ curves under different discharge

3. Analysis of cavitating flows

3.1 Unsteady cavity behavior under low flow rate condition

Figure 3 illustrates the general development of cavities in the impeller channels with the decrease of the *NPSH* corresponding to the above five points for 0.7*Q*o. The regions experiencing cavitation appear in orange (where the iso-surface value is 0.05) in the images. As *NPSH* decreases, cavities first appear on the leading edge of the blades near the hub (Cond. B), the zone of cavitation then extends downstream, and expand more near the hub side than the shroud side (Cond. C). Then, the cavities grow dramatically in length (Cond. D and E) and form major blockages in the upstream of the inter-blade channels. It can be seen from Cond. C, D and E that the size and shape of the cavities in each channel are different, and among the three conditions the differences are much more obvious in Cond. C. Such observations closely agree with the calculation results available in the literature Leroux *et al.* (2005), which may arise from the asymmetry of interior field of pump because of interaction between impeller and tongue (Jeanty *et al.*, 2009). This hypothesis will be analyzed in detail in the following sections, and the reason will be addressed.

3.1.1 Unsteady cavity behavior in one evolution cycle. As indicated above, for flow rate 0.7*Q*o, the size and shape of cavities in each channel are qualitatively different between Cond. B and Cond. C. It was also found (not surprisingly) that the period of one cavity evolution cycle was exactly equal to the impeller rotation period. This implies that the shedding frequency is quite different from that in the hydrofoil cavitation tests, and that the change is associated with the strong interference of the uneven flow distribution near the tongue. The evolution of cavitation bubbles inside the impeller under this condition are shown in Figure 4 for $t = 0$, T/6, …, 5/6*T*. In these images, one blade ("Blade1") is shown and the flow channel on the suction side of Blade 1 was named as "Ch.1" and highlighted with red circle. To a casual glance these six images

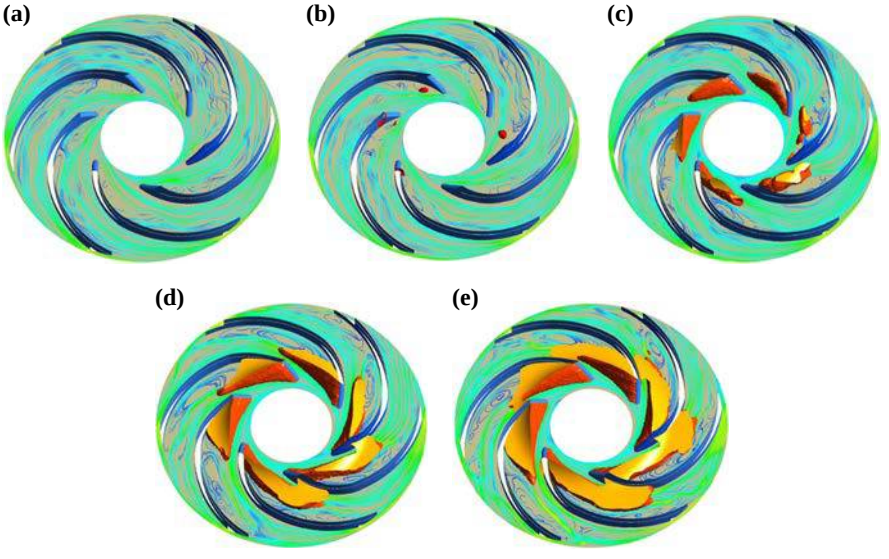

Figure 3.
Cavity development in the impeller channels with the decrease of *NPSH* (0.7*Q*o)

Notes: (a) Cond. A; (b) Cond. B; (c) Cond. C; (d) Cond. D; (e) Cond. E

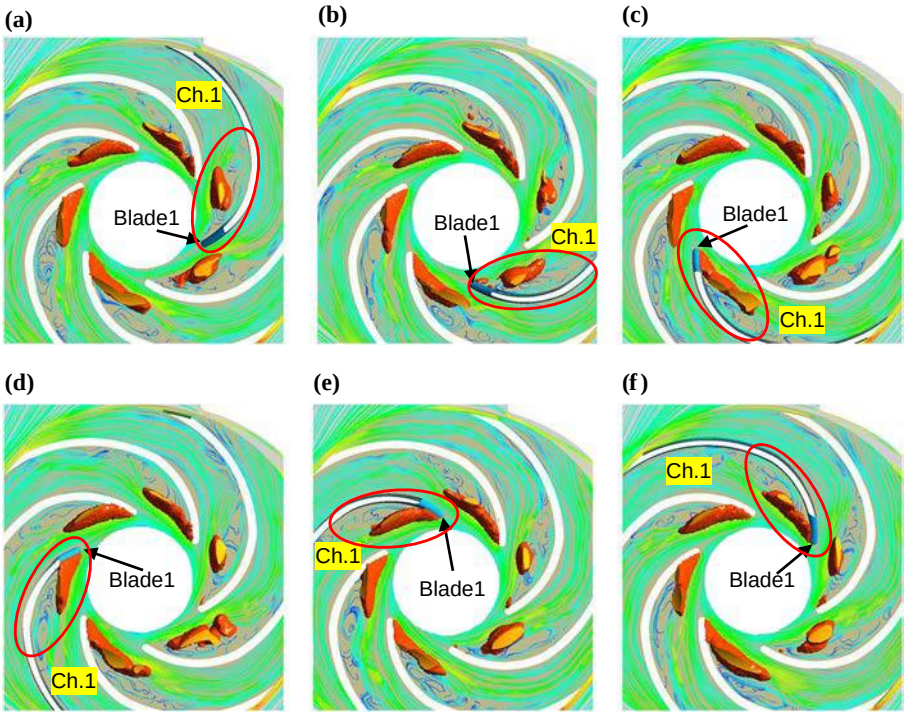

Notes: (a) $\theta = 0°$, $t = 0$; (b) $\theta = 120°$, $t = \frac{1}{6}T$; (c) $\theta = 120°$, $t = \frac{2}{6}T$; (d) $\theta = 180°$, $t = \frac{3}{6}T$; (e) $\theta = 240°$, $t = \frac{4}{6}T$; (f) $\theta = 300°$, $t = \frac{5}{6}T$

Figure 4.
Cavity evolution and velocity distribution in the middle section (Cond. C, 0.7Q_o)

look almost the same; however, a careful inspection of the cavity in one single channel, for example Ch.1, makes the cavity evolution cycle quite obvious.

To better explain this, the location where the trailing edge of "Blade1" reaches to the volute tongue is defined the angle $\theta = 0°$, as shown in Figure 4(a). The periodic cavity development in one rotation period (from $\theta = 0°$ to $\theta = 360°$) can be divided into three stages. At the $\theta = 0°$ position a small cavity is seen attached to leading edge of the blade together with a large separated cavity (formed in the previous cycle) detached in the flow channel. Over the stages of cavity growth ($\theta = 0°$-60°-120°), the leading edge cavity grows and eventually merges with separated cavity in the rear part to form a narrow cavity as the blade moving away from the volute tongue. Soon after the contraction stage occurs (120°-180°-240°), during which the cavity become shorter but thicker. Finally when the blade again approaches the tongue (240°-360° (0°)), the cavity separates into two parts which completes the evolution over one cycle. It can also be found that the cavity evolution processes in other passages are nearly identical with that in "Ch.1", and the cavity shape is functionally equivalent at each blade-tongue position.

The pressure fluctuations of the monitoring points are also recorded for all the five conditions. Figure 5 compares the pressure fluctuations under Cond. C with Cond. A. As can be seen, the first appearance of the cavities coincides with a decrease in

pressure at all monitoring points, but particularly at points ps1 and ss1, when a bubble passed through the monitoring point, the pressure is steady for a short while, leading to the clipped or cutoff appearance of the graph. However, the period is unchanged and the first order frequency remains at the rotational frequency (48.8 Hz). This observation agrees nicely with previous discussion that the shedding frequency inside the pump is same with the rotational frequency, in contrast to what is observed in hydrofoil tests.

3.1.2 Influence of impeller-tongue interaction on the unsteady cavity behavior. As observed in many hydrofoil cavitating flow experiments, adverse pressure gradients in the trailing part of the cavity accounts for the formation of the reversed flow. At off-design points, the pressure distribution in the runner is non-uniform in six channels. For the 0.7*Q*o condition, when the channel rotates to the tongue, the reverse pressure gradient will be larger than in other locations and thus the reverse flow increases in severity. The following analysis shows that the impeller-tongue interaction and non-uniform pressure distribution in the volute are the main causes for the periodic change of cavities.

The pressure distribution in the volute for flow rate 0.7*Q*o Cond. C is shown in Figure 6(b). The cavity evolution in Figure 4 indicates that the flow structure in

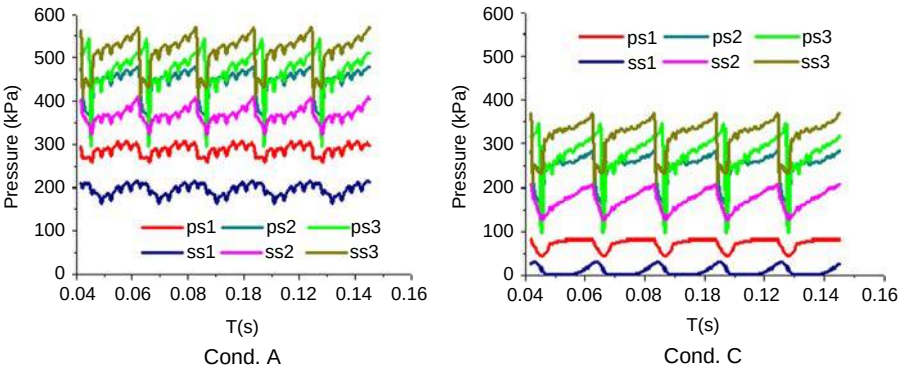

Figure 5.
The comparison of pressure pulsation amplitude under Cond. A and Cond. C

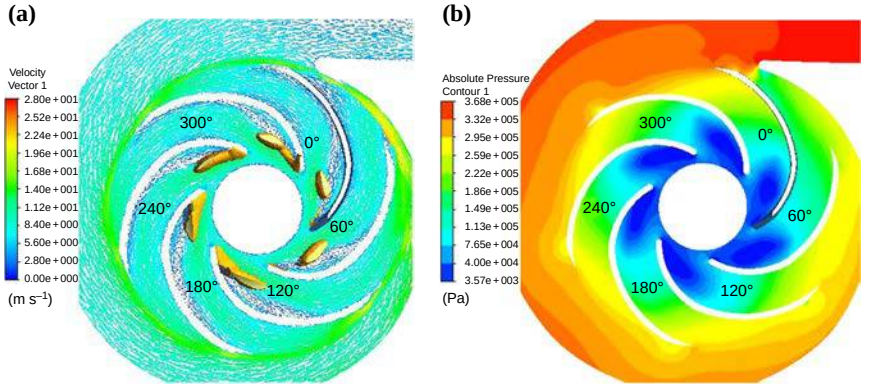

Figure 6.
Cavity and pressure distribution in the middle plane section of impeller (Cond. C, 0.7*Q*o)

Notes: (a) Cavity and velocity vectors; (b) pressure distribution

the blade-tongue position is always similar. Thus, the pressure within any of the six channels in Figure 6(b) can be used to represent the pressure distribution during one revolution. Combining this pressure distribution with the cavities in Figure 6(a), which was at the same time as in Figure 4(a), a detailed account can be provided: as shown in Figure 6(b), the pressure in cavitation region is lower than the saturated pressure and the pressure in the volute is non-uniform. Again take the highlighted "Blade1" and "Ch.1" as an example, the outlet pressure is lower in cavity growth stage (0°-60°-120°) which means the exit pressure and vortex region decreases as the blade passes the tongue, and then the vortex core moves a little toward the blade exit in response to the pressure gradient. Hence the two separated cavities grow and merge.

Then as "Blade1" moves away from the tongue, the exit pressure for "Ch.1" increases gradually (over positions 120°-180°-240°). The higher pressure in the rear part of the cavity causes condensation of the vapor. These effect results in the cavities looking a little shorter and thicker in the 180° position. During this stage, reversed flow can be observed but is insufficiently developed to cause separation of the cavity.

In the separation stage (240°-300°-0°), the impeller exit pressure increases greatly as the blades move toward the tongue. The vapor condensation rate thus increases. Severe reversed flow can now be seen near the suction of the blade and it gradually extends as far as the leading edge. This perturbation eventually cuts the majority of the cavity from the blade. The presence of this reversed flow has been discussed by many researchers in the context of both inducers and hydrofoils. The reverse flow was indicated to have significance effects on the shedding of large cavity structure (Coutier-Delgosha *et al.*, 2003; Tani *et al.*, 2012), which is further confirmed in this centrifuge pump case.

Above analysis strongly argues that two main facts are essential for the cavity evolution mechanism in the pump case: one is importance of the impeller-tongue interaction caused by the rotation of the rotor, the other is the associated non-uniform pressure distribution in the volute. These two realities together result in a periodic change of pressure at the flow passage exit, causing a forced life cycle of the cavity in the flow passage.

In Figure 3, periodic growth-contraction life cycle can also be seen for Cond. D and Cond. E. However, no separation of the cavity is observed in these cases. This is probably accounted for by the greater thickness of the cavity in these more severe cases meaning that there is too little for condensation to produce two separate regions.

For even lower flow rate 0.46Qo, the life cycles were quite similar with that for 0.7Qo. Thus the lower flow case is not presented or discussed in detail here.

The combination of the two effects of impeller-tongue interaction and non-uniform pressure distribution in the volute on the evolution of cavities in the impeller channels were further verified by results at optimal and large flow rate conditions, which are presented below.

3.2 Results for flow rate 1.0Qo and 1.3Qo

With the decrease of *NPSH*, the cavitation development for flow rate 1.0Qo and a large flow rate 1.3Qo show the same general characteristics as with the reduced 0.7Qo flow. With the larger flows, small cavities again first appear on the leading edge then extend both downstream and laterally.

Since the cavity is almost identical in the same blade-tongue position, the cavity shape and the flow pattern at $t = 0$, T/6, …, 5/6T are almost the same. So only images at $t = 0$ are shown in Figures 7 and 8 for another two flow rate 1.0Qo and 1.3Qo.

For optimal condition 1.0Qo the pressure distribution in volute is relatively symmetrical (see Figure 7). Even with the rotation of the impeller, the cavity shape on each channel remains almost the same. That means the cavity is relatively stable during one rotation period.

However, for the larger flow rate 1.3Qo, it can be found that the cavity in one rotation period experiences two primary stages. Unlike the condition 0.7Qo, the growth stage is in the region of 240°-300°-0° (Figure 8), corresponding to the low pressure area in the volute. This is followed by a contraction stage (0°-60°-120°-180°) in which the cavity shortens and thickens with a small amount of shedding along its trailing edge. This was caused by combination effects of high exit pressure in the volute and vortex movements in the rear. The mechanism of this phenomenon is similar with 0.7Qo, which is caused by the alternating interaction between reverse flow and cavity

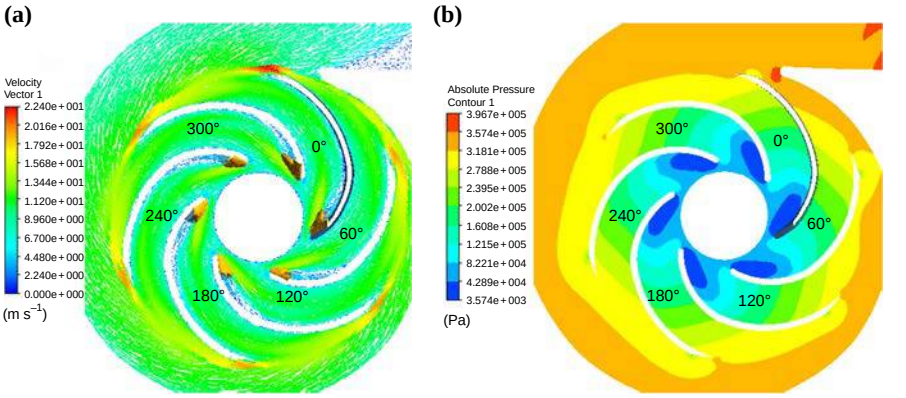

Notes: (a) Cavity and velocity vectors; (b) pressure distribution

Figure 7.
Cavity and pressure distribution in the middle plane section of impeller (Cond. C, 1.0Qo)

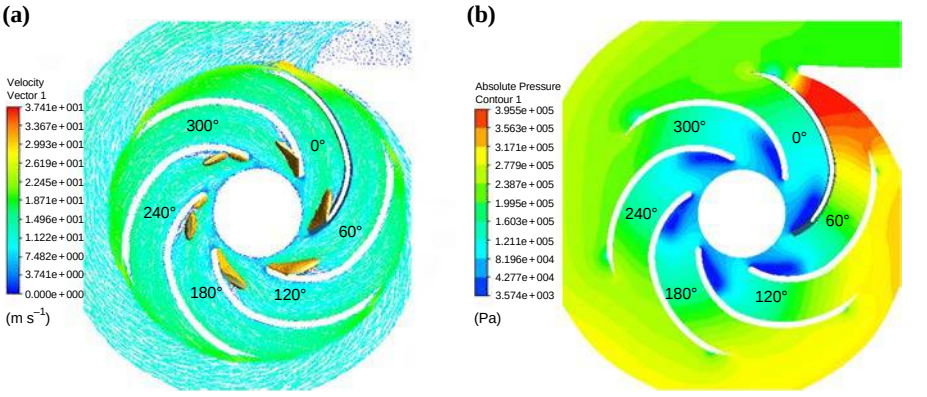

Notes: Cavity and velocity vectors; (b) pressure distribution

Figure 8.
Cavity and pressure distribution in the middle plane section of impeller (Cond. C, 1.3Qo)

interface due to the impeller-tongue interaction and the uneven pressure distribution in volute, as shown in Figure 8.

3.3 Summary of cavitation under different flow rates

It is noticeable that for large flow rate condition, the majority of the cavity is attached to the suction side of the blade, while for low flow rate and optimal condition, the cavity attaches to the blade suction side near the leading edge and eventually migrates to the middle of the passage. The large positive attack angle under low discharge condition and a small negative attack angle under high flow rate condition is the main reason for this difference. In fact, the different cavity evolution cycle at above three flow rate is also related to the different attacking angle.

As shown in Figure 9, at low flow rate 0.7*Q*o, there exist large positive attacking angle and a vortex region is observed in each channel near the suction side even without cavitation (Cond. A). In Cond. C with the influence of high reverse pressure gradient in highlighted channel, the vortex core moves toward the blade leading edge and the reversed flow velocity magnitude is greatly increased comparing with that in Cond. A, which cut the cavity into two parts in the highlighted channel.

Since the pressure distributions in the volute are different for low flow rate and large flow rate case, the cavity growth and contraction stage occur in different blade-tongue positions for the two cases. For the optimal flow condition, the cavities are relatively stable and the pressure distribution is strongly symmetrical, and thus there is only a small difference between each channel.

For the low flow rate off-design points in Cond. C, the cavities show obvious life cycle including growth, contraction, separation and collapse with a frequency equal to the rotational rate of the impeller. As has been observed in many hydrofoil cavitating flow experiments, the interaction between reverse flow and cavity interface is the main reason leading to cavity separation. However, unlike the self-excited cloud generation in the hydrofoil case, the combined effect of uneven pressure distribution in the volute and impeller-tongue interaction is the main reason for the periodic evolution of the cavities; periodic growth-contraction life cycle can also be seen for Cond. D and Cond. E. However, no separation of the cavity is observed, likely associated with the greater extent of cavitation in these cases.

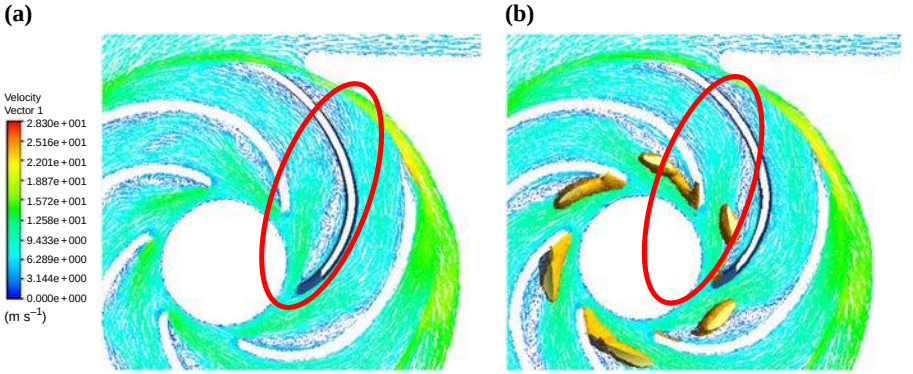

Figure 9.
Velocity distribution in Ch.1 at $t = 0$ (0.7*Q*o)

Notes: (a) Cond. A; (b) Cond. C

4. Conclusion

Unsteady three-dimensional cavitating flow field in a centrifugal pump is simulated using Zwart-Gerber-Belamri cavitation model and RNG $k-\varepsilon$ turbulence model. The *NPSH-H* curve and the cavitation development in the whole passage were predicted. Following conclusions are evident:

With the decrease of the outlet pressure (thus *NPSH*), small cavities first appear on the leading edge of the blades near hub (Cond. B). The cavities then grow downstream and extend more quickly toward the hub than toward shroud (Cond. C). After this, the cavity quickly lengthen and thicken (Cond. D and E) and strongly blockages the inter-blade channels, leading to a choking condition.

Unsteady cavitating flow under various flow conditions are analyzed: reverse flow caused by the impeller-tongue interaction is the main reason for making the periodic of cavities inside a pump, making it quite different from the hydrofoil case in this sense. The differences in cavitating bubble distribution are also analyzed, the attack angle lead to the difference between different flow rate conditions. And the pressure distribution under different flow rate conditions also result in different locations where cavity growth and contraction stage take place.

References

ANSYS (2012), "ANSYS CFX-Solver Theory Guide", ANSYS CFX, Release11.0, pp. 69-118.

Coutier-Delgosha, O., Fortes-Patella, R., Reboud, J.L. and Pouffary, B. (2002), "3D numerical simulation of pump cavitating behavior", *ASME 2002 Joint US-European Fluids Engineering Division Conference*, *Montreal*, pp. 815-824.

Coutier-Delgosha, O., Fortes-Patella, R., Reboud, J.L., Stoffel, B. and Hofmann, M. (2003), "Experimental and numerical studies in a centrifugal pump with two-dimensional curved blades in cavitating condition", *Journal of Fluids Engineering*, Vol. 125 No. 6, pp. 970-978.

Coutier-Delgosha, O., Reboud, J.L. and Fortes-Patella, R. (2002), "Numerical study of the effect of the leading edge shape on cavitation around inducer blade sections", *JSME International Journal Series B*, Vol. 45 No. 3, pp. 678-685.

Dupont, P. and Casartelli, E. (2002), "Numerical prediction of the cavitation in pumps", *ASME 2002 Joint US-European Fluids Engineering Division Conference*, *Montreal*, pp. 825-833.

Flores, N.G., Goncalvès, E., Patella, R.F., Rolland, J. and Rebattet, C. (2008), "Head drop of a spatial turbopump inducer", *Journal of Fluids Engineering*, Vol. 130 No. 11, pp. 111301-1-111301-10.

Hao, Z.R., Wang, L.Q. and Wu, D.Z. (2010), "Numerical simulation of unsteady cavitating flow on hydrofoil", *Journal of Zhejiang University*, Vol. 44 No. 5, pp. 1044-1048.

Huang, B., Wang, G.Y. and Han, Z.Z. (2010), "Study on the cavitating flow around the blunt axisymm etric body", *Science Technology and Engineering*, Vol. 110 No. 4, pp. 8730-8735.

Huang, B., Wang, G.Y. and Quan, X.B. (2011), "Study on the unsteady cavitating flow dynamic characteristics around a 0-caliber ogive revolution body", *Journal of Experiments in Fluid Mechanics*, Vol. 25, pp. 22-28.

Huang, B., Wang, G.Y. and Wang, F.F. (2011), "Experimental investigation on flow field structure of unsteady cavitation flow", *Journal of Experimental Mechanics*, Vol. 26 No. 4, pp. 417-424.

Jeanty, F., Andrade, J.D., Asuaje, M., Kenyery, F., Vásquez, A., Aguillón, O. and Tremante, A. (2009), "Numerical simulation of cavitation phenomena in a centrifugal pump", *ASME 2009 Fluids Engineering Division Summer Meeting*, pp. 331-338.

Kobayashi, K. and Chiba, Y. (2009), "Numerical simulation of cavitating flow in mixed flow pump with closed type impeller", *ASME 2009 Fluids Engineering Division Summer Meeting. American Society of Mechanical Engineers*, pp. 339-347.

Leroux, J.B., Delgosha, O.C. and Astolfia, J.A. (2005), "A joint experimental and numerical study of mechanisms associated to instability of partial cavitation on two-dimensional hydrofoil", *Physics of Fluids*, Vol. 17 No. 5, pp. 052101-052120.

Li, J., Liu, L.J. and Li, G.J. (2007), "Numerical prediction of cavitation flows in a centrifugal pump impeller", *Journal of Engineering Thermophysics*, Vol. 28 No. 6, pp. 948-950.

Medvitz, R.B., Kunz, R.F., Boger, D.A., Lindau, J.W., Yocum, A.M. and Pauley, L.L. (2002), "Performance analysis of cavitating flow in centrifugal pumps using multiphase CFD", *Journal of Fluids Engineering*, Vol. 124 No. 2, pp. 377-383.

Mejri, I., Bakir, F., Rey, R. and Belamri, T. (2005), "Comparison of computational results obtained from a VOF cavitation model with experimental investigations of three inducers: Part I–experimental investigations; Part II–numerical analysis", *ASME 2005 Fluids Engineering Division Summer Meeting. American Society of Mechanical Engineers*, pp. 1147-1191.

Mejri, I., Bakir, F., Rey, R. and Belamri, T. (2006), "Comparison of computational results obtained from a homogeneous cavitation model with experimental investigations of three inducers", *Journal of Fluids Engineering*, Vol. 128 No. 12, pp. 1308-1323.

Niazi, E., Mahjoob, M.J. and Bangian, A. (2010), "Experimental and numerical study of cavitation in centrifugal pumps", *ASME 2010 10th Biennial Conference on Engineering Systems Design and Analysis. American Society of Mechanical Engineers*, pp. 395-400.

Nwaoha, C. (2009), "Cavitation control in centrifugals", *World Pumps*, Vol. 2009 No. 519, pp. 22-24.

Okita, K., Matsumoto, Y. and Kamijo, K. (2003), "Numerical analysis for unsteady cavitating flow in a pump inducer", *5th International Symposium on Cavitation, Osaka, November*.

Pouffary, B., Patella, F.R., Reboud, J.L. and Lambert, P.A. (2008a), "Numerical analysis of cavitation instabilities in inducer blade cascade", *Journal of Fluids Engineering*, Vol. 130 No. 4, pp. 1-8.

Pouffary, B., Patella, R.F., Reboud, J.L. and Lambert, P.A. (2008b), "Numerical simulation of 3D cavitating flows: analysis of cavitation head drop in turbomachinery", *Journal of Fluids Engineering*, Vol. 130 No. 6, pp. 061301-1-061301-10.

Tani, N., Yamanishi, N. and Tsujimoto, Y. (2012), "Influence of flow coefficient and flow structure on rotational cavitation in inducer", *Journal of Fluids Engineering*, Vol. 134 No. 2, pp. 1-13.

Wang, G.Y., Cao, S.L. and Ikohagi, T. (2001), "Vortex cavitation mechanisms in shear layer flow", *Journal of Tsinghua University*, Vol. 41 No. 10, pp. 62-64.

Watanabe, S., Inoue, N. and Ishizaka, K. (2009), "A study on back flow structure in a 2-blade helical inducer at a partial flow rate", *ASME 2009 Fluids Engineering Division Summer Meeting*, pp. 267-275.

Xiao, Y.X., Wang, Zh. W., Yan, Z.G., Li, M.G., Xiao, M. and Liu, D.Y. (2010), "Numerical analysis of unsteady flow under high-head operating conditions in Francis turbine", *Engineering Computations*, Vol. 27 No. 3, pp. 365-386.

Corresponding author
Lingjiu Zhou can be contacted at: zlj09@263.net